

Intensity-dependent control of dissociation pathways in strong-field double ionization of ethylene

Jianting Lei(雷建廷), Luqi Li(李潞琪), Xiangjie Chen(陈祥杰), Chenyu Tao(陶琛玉), Shuncheng Yan(闫顺成), Qingcao Liu(刘情操), and Shaofeng Zhang(张少锋)

Citation: Chin. Phys. B, 2026, 35 (**4**): 043301. DOI: 10.1088/1674-1056/ae3608
http://cpb.iphy.ac.cn; http://iopscience.iop.org/cpb

What follows is a list of articles you may be interested in

Photoelectron momentum distributions of triatomic CO_2 molecules by circularly polarized attosecond pulses

Si-Qi Zhang(张思琪), Jun Zhang(张军), Xin-Yu Hao(郝欣宇), Jing Guo(郭静), Aihua Liu(刘爱华), and Xue-Shen Liu(刘学深)

Chin. Phys. B, 2024, 33 (**10**): 103301. DOI: 10.1088/1674-1056/ad6b81

Ultrafast Coulomb explosion imaging of molecules and molecular clusters

Xiaokai Li(李孝开), Xitao Yu(余西涛), Pan Ma(马盼), Xinning Zhao(赵欣宁), Chuncheng Wang(王春成), Sizuo Luo(罗嗣佐), and Dajun Ding(丁大军)

Chin. Phys. B, 2022, 31 (**10**): 103304. DOI: 10.1088/1674-1056/ac89df

Geometric structure of N_2O^{q+} (q = 5, 6) studied by Ne^{8+} ion-induced Coulomb explosion imaging

Xi Zhao(赵曦), Xu Shan(单旭), Xiaolong Zhu(朱小龙), Lei Chen(陈磊), Zhenjie Shen(沈镇捷), Wentian Feng(冯文天), Dalong Guo(郭大龙), Dongmei Zhao(赵冬梅), Ruitian Zhang(张瑞田), Yong Gao(高永), Zhongkui Huang(黄忠魁), Shaofeng Zhang(张少锋), Xinwen Ma(马新文), and Xiangjun Chen(陈向军)

Chin. Phys. B, 2021, 30 (**11**): 113302. DOI: 10.1088/1674-1056/abff45

Direct Coulomb explosion of N_2O^{2+} induced by monochromatic extreme ultraviolet photons at 38.5 eV

Min Zhang(张敏), B Najjari, Bang Hai(海帮), Dong-Mei Zhao(赵冬梅), Jian-Ting Lei(雷建廷), Da-Pu Dong(董达谱), Shao-Feng Zhang(张少锋), Xin-Wen Ma(马新文)

Chin. Phys. B, 2020, 29 (**6**): 063302. DOI: 10.1088/1674-1056/ab8629

Coulomb explosion of CS_2 molecule under an intense femtosecond laser field

Xiao Wang(王潇), Jian Zhang(张健), Shi-An Zhang(张诗按), Zhen-Rong Sun(孙真荣)

Chin. Phys. B, 2016, 25 (**5**): 053301. DOI: 10.1088/1674-1056/25/5/053301

SPECIAL TOPIC — Ultrafast physics in atomic, molecular and optical systems

Intensity-dependent control of dissociation pathways in strong-field double ionization of ethylene

Jianting Lei(雷建廷)[1,2,†], Luqi Li(李潞琪)[1,5,†], Xiangjie Chen(陈祥杰)[1], Chenyu Tao(陶琛玉)[2,3], Shuncheng Yan(闫顺成)[2,3], Qingcao Liu(刘情操)[1,‡], and Shaofeng Zhang(张少锋)[2,3,4,§]

[1] *College of Science, Harbin Institute of Technology, Weihai* 264209, *China*
[2] *Institute of Modern Physics, Chinese Academy of Sciences, Lanzhou* 730000, *China*
[3] *University of Chinese Academy of Sciences, Beijing* 100049, *China*
[4] *State Key Laboratory of Heavy Ion Science and Technology, Lanzhou* 730000, *China*
[5] *School of Physics, Harbin Institute of Technology, Harbin* 150001, *China*

(Received 11 November 2025; revised manuscript received 7 January 2026; accepted manuscript online 9 January 2026)

We investigate the dissociation dynamics of ethylene (C_2H_4) in strong femtosecond laser fields using a reaction microscope. Coincidence ion detection enables reconstruction of fragment momenta and identification of multiple two-body channels of $C_2H_4^{2+}$, including $C_2H_3^+ + H^+$, $CH_2^+ + CH_2^+$, and $C_2H_2^+ + H_2^+$. Particular attention is given to the symmetric $CH_2^+ + CH_2^+$ channel. With increasing laser intensity, the kinetic energy release peak shifts from 5.2 eV to 7.3 eV, indicating a transition from dissociation via lower excited states (e.g., $^3B_{3u}$ and ^1A_u (S_2)) to higher-lying states (e.g., ^3Ag and $^1B_{3g}$). The observed evolution of state populations highlights that peak laser power density governs the selection of dissociation pathways. By tuning laser parameters, specific channels can be enhanced or suppressed, providing an effective approach for steering molecular fragmentation dynamics in polyatomic systems.

Keywords: coincidence measurement, kinetic energy release (KER), Coulomb explosion

PACS: 33.80.–b, 33.80.Rv, 34.50.–s, 34.50.Lf, 07.77.–n

DOI: 10.1088/1674-1056/ae3608 **CSTR:** 32038.14.CPB.ae3608

1. Introduction

Laser-induced dissociation dynamics of polyatomic molecules stands as a core frontier in atomic and molecular physics, linking fundamental theory to practical applications.[1–5] In strong laser fields, molecular dissociation entails chemical bond cleavage, atomic rearrangement, ultrafast electronic state transitions, and coupled electronic-nuclear dynamics.[6–11] Recent advances in ultrafast laser and imaging techniques have enabled real-time tracking of bond evolution on femtosecond to attosecond scales,[10,12,13] advancing our understanding of microscopic dissociation processes and supporting applications in interstellar chemistry,[14,15] atmospheric reactions,[16,17] and notably, quantum control of molecular processes.[18,19] A critical unmet need, however, lies in clarifying intensity-dependent control mechanisms for polyatomic systems such as ethylene, building on insights from simpler molecules.

Strong laser fields offer a direct means to excite and manipulate intramolecular electronic motion, with the central challenge of laser-induced dissociation being the precise control of ionic quantum states to steer fragmentation pathways. Laser parameters (intensity, frequency, pulse duration) critically regulate electronic state distribution and dissociation outcomes,[20–22] enabling targeted manipulation of fragmentation channels. For diatomic molecules, two key electronic state preparation pathways have been established: (i) sub-cycle ionization, where ultrafast pulses remove inner-valence electrons to directly populate high-lying ionic states governing post-pulse nuclear dynamics;[2,23,24] and (ii) outer-valence electron ionization, which initially populates low-lying states that are subsequently field-excited to dissociative higher states.[25,26] Extending this understanding to intensity-dependent control in ethylene remains an urgent research gap, which this study addresses.

Hydrocarbons are ubiquitous in nature and industry and have long served as targets for experimental studies. Ethylene (C_2H_4), a common hydrocarbon and feedstock for many organic syntheses, has been a primary focus for studying dissociation processes. A variety of experimental techniques have been employed to probe the ionization and fragmentation of C_2H_4, including double charge transfer spectroscopy,[27] TOF mass spectrometry,[28] and Auger spectroscopy.[29,30] Gaire *et al.*[31] conducted the first kinematically complete direct single-photon double ionization measurements of C_2H_4 near

[†]These authors contributed equally to this work.
[‡]Corresponding author. E-mail: qingcao.liu@hit.edu.cn
[§]Corresponding author. E-mail: zhangshf@impcas.ac.cn

© 2026 Chinese Physical Society and IOP Publishing Ltd. All rights, including for text and data mining, AI training, and similar technologies, are reserved.

the double-ionization threshold, and quantum-chemical calculations were used to propose the electronic states and excitation pathways associated with different dissociation channels of $C_2H_4^{2+}$. Building on this, Jochim *et al.*[32] introduced a method to extract transient metastable lifetimes and reconstruct the full three-dimensional momentum of dissociation fragments, focusing on the deprotonation channel $C_2H_4^{2+} \rightarrow C_2H_3^+ + H^+$. They reported lifetimes of 202 ± 10 ns and 916 ± 40 ns for this channel, with corresponding values of 269 ± 29 ns and 956 ± 83 ns in C_2D_4. To gain a more comprehensive understanding of the dissociation dynamics, Wang *et al.*[33] investigated the two-body and three-body fragmentation channels of $C_2H_4^{2+}$ using 300 eV electrons combined with ion–ion coincidence detection, obtaining KER distributions and reconstructing initial-state information for each channel. For three-body fragmentation, Newton-diagram features indicated that a two-step sequential mechanism dominates: $C_2H_4^{2+}$ first undergoes two-body breakup, followed by delayed loss of a neutral H atom from the intermediate cation ($C_2H_3^+$, $C_2H_2^+$, or CH_2^+). In parallel, studies on the C_2H_4 dimer system by Kalugina *et al.*[34] focused on intermolecular interactions. Using *ab initio* and analytical approaches, they systematically mapped the PES and dipole moments of the $(C_2H_4)_2$ and showed that for intermolecular separations larger than 11 a_0, a long-range model accurately captures the interaction energy and induced dipole. Despite these extensive efforts, previous studies have largely concentrated on processes induced by high-energy particles or photons. In contrast, strong-field laser–induced double ionization of C_2H_4 typically involves simultaneous population of multiple electronic states; the corresponding state-evolution pathways and their quantitative relation to field strength remain insufficiently clarified. As a result, the control of C_2H_4 double-ionization dissociation pathways under intense laser fields remains largely unexplored.

In this work, we investigate the dissociation dynamics of $C_2H_4^{2+}$ in strong laser fields using coincidence imaging techniques. Experimentally, we observed multiple fragmentation channels, including $C_2H_3^+ + H^+$, $CH_2^+ + CH_2^+$, and $C_2H_2^+ + H_2^+$. Combined with theoretical analysis, we elucidate the initial electronic states and dissociation mechanisms underlying these channels, with particular emphasis on the intensity-dependent regulation of the symmetric dissociation channel ($CH_2^+ + CH_2^+$) over a laser intensity range of 1×10^{14}–2×10^{15} W/cm^2. Our results demonstrate that the laser power density significantly influences the excitation probability of specific electronic states and the subsequent fragmentation dynamics. This deepens our understanding of controlling the breakup of polyatomic molecules.[23,35,36]

2. Experimental apparatus

The experimental platform consists of a reaction microscope coupled to a Ti:sapphire femtosecond laser system. The laser delivers pulses with a center wavelength of 790 nm, a duration of 25 fs, a repetition rate of 3 kHz, and single-pulse energies up to 3 mJ. After focusing with a 15 cm focal-length lens, the beam is directed perpendicularly into the supersonic cold-target region of the reaction microscope, where it interacts with a jet of C_2H_4 molecules. The laser intensity was determined by measuring the yield variation of Ar^+ and Ar^{2+} ions as a function of laser intensity and comparing the measured Ar^+ ion yield with theoretical results calculated using the ADK theory.[37] The laser intensities used in the experiments were calibrated to be 1×10^{14} W/cm^2 and 8×10^{14} W/cm^2. The reaction microscope comprises a multistage differentially pumped supersonic source, an ultra-high-vacuum (UHV) interaction chamber, a time-of-flight (TOF) mass-spectrometry section, and a time- and position-sensitive detector. During operation, C_2H_4 at 1 bar is expanded through a 30 μm nozzle into the source chamber and is subsequently collimated by a skimmer and apertures before entering the UHV target region. In the interaction zone, the focused femtosecond pulses cross the molecular beam, producing ionic fragments. The fragments are accelerated by uniform extraction fields along a defined axis and recorded by the time- and position-sensitive detector. By measuring the arrival time and impact position of each ion, we reconstruct the full three-dimensional momentum vectors of all fragments detected in coincidence. The target density at the laser focus is carefully controlled to ensure that only one C_2H_4 molecule interacts with each laser pulse. This condition guarantees that all electrons and ionic fragments detected per shot originate from the same parent molecule, allowing for clear channel assignments. Due to the precise three-dimensional momentum resolution of the reaction microscope, we observe abundant parent dications ($C_2H_4^{2+}$) in the strong-field double-ionization experiments. Under linearly polarized light, the process is dominated by nonsequential double ionization, where removal of two electrons from the HOMO prepares a relatively long-lived ground-state dication, which can be directly detected in the spectrometer.

3. Analysis and discussion

Using ion–ion coincidence measurements, we recorded fragment-ion pairs produced in the dissociation of C_2H_4 at a peak laser intensity of 1×10^{14} W/cm^2. Figure 1 presents the two-dimensional TOF correlation map of fragments following double ionization of C_2H_4. Because momentum is conserved during the Coulomb explosion, distinct reaction channels manifest as narrow linear features with characteristic slopes. Four

principal channels are clearly resolved: the deprotonation channel $C_2H_3^+ + H^+$, the H_2^+ channel $C_2H_2^+ + H_2^+$, and the symmetric cleavage $CH_2^+ + CH_2^+$. Notably, the $C_2H_3^+ + H^+$ channel exhibits an island-like cluster with a pronounced trailing tail in the correlation map. This structure originates from long-lived metastable ionic intermediates,[25] highlighting the distinctive kinetics associated with such states.

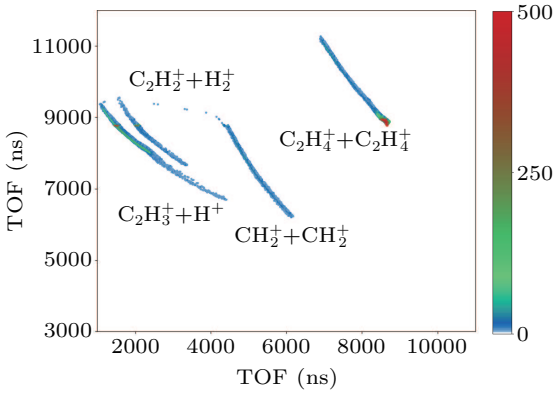


Fig. 1. TOF correlation map for the dissociation of C_2H_4 molecules induced by an 800 nm femtosecond laser at 1×10^{14} W/cm^2.

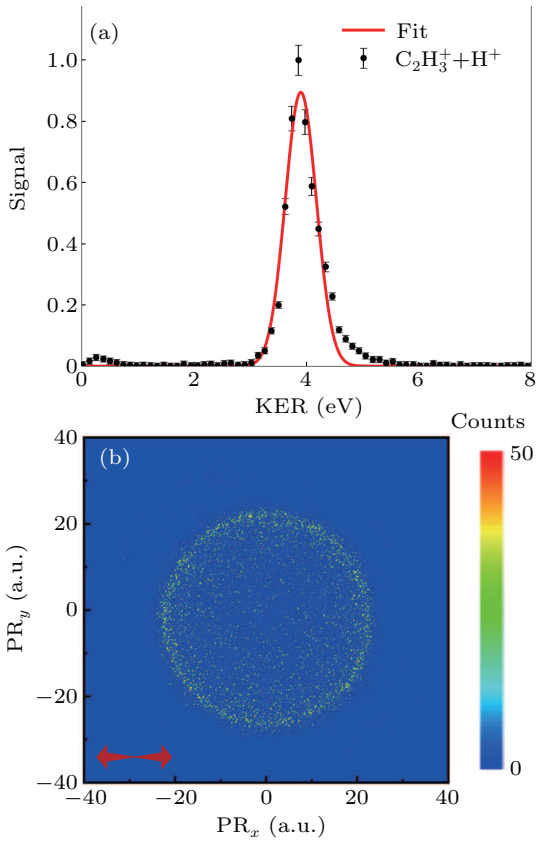


Fig. 2. Dissociation channel of $C_2H_3^+ + H^+$: (a) KER spectrum; (b) 2D momentum distribution of H^+ in the x, y-plane.

Figure 2(a) shows the KER spectrum of the deprotonation dissociation channel $C_2H_4^{2+} \rightarrow C_2H_3^+ + H^+$. The spectrum exhibits a narrow distribution with a peak around 3.8 eV. Figure 2(b) presents the two-dimensional momentum distribution of H^+ ions in the xy plane. P_R represents the recoil ion momentum, where the x direction corresponds to the laser polarization and the y direction corresponds to the laser propagation direction. It is evident that the fragment ions are isotropically distributed, indicating that the angular distribution of fragments from the deprotonation channel of C_2H_4 shows no directional dependence. This phenomenon suggests that the separation of the two fragment ions through Coulomb explosion occurs on a timescale longer than the rotational period of the molecule in space after the laser pulse has ceased.

According to the potential energy curves along the C–H bond coordinate,[31] when one electron from the HOMO–1 orbital and one from the HOMO orbital are ionized, the resulting $C_2H_4^{2+}$ ion can populate the lowest electronically excited state ^3A_u (T_1), which leads to C–H bond cleavage with a KER of approximately 3.7 eV. It is worth noting that the KER distribution in Fig. 2(a) exhibits a high-energy tail, which corresponds to dissociation from the ^1A_u (S_2) state, where the potential energy surface predicts a KER of approximately 4.3 eV. Furthermore, along the C–H coordinate, the potential energy surface features a shallow yet extended barrier. Consequently, this state exhibits a relatively long lifetime, and the dissociation of $C_2H_4^{2+}$ along the C–H bond proceeds slowly, which accounts for the isotropic angular distribution of the product ions.

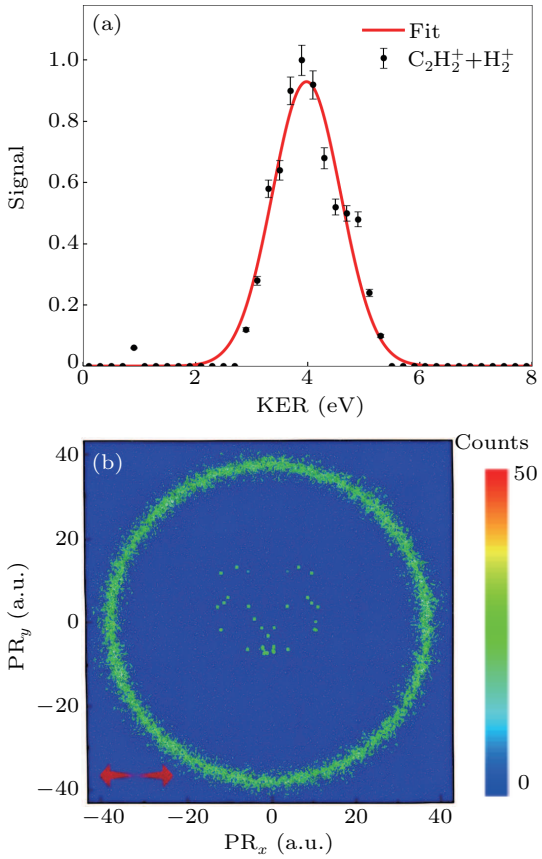


Fig. 3. KER spectrum of the $C_2H_4^{2+} \rightarrow C_2H_2^+ + H_2^+$ reaction channel. (a) KER spectrum; (b) 2D momentum distribution of H_2^+ in the x, y-plane.

As shown in Fig. 3(a), the KER spectrum for the $C_2H_4^{2+} \rightarrow C_2H_2^+ + H_2^+$ channel peaks at approximately 4 eV. This channel exhibits an isotropic angular distribution

(Fig. 3(b)), which originates from its dominant dissociation pathway and specific features of the potential energy surface. The H_2^+ formation proceeds mainly via two plausible pathways: (1) migration of a hydrogen atom across the C=C bond, forming an ethyl-like cationic intermediate (CH_3CH^{2+}) that subsequently fragments into $HCCH^+$; or (2) recombination of two hydrogen atoms on the same carbon, followed by separation from the vinylidene ion (CH_2C^+). Given that pathway (1) necessitates a long-distance proton transfer across the double bond, it follows that pathway (2) becomes the dominant route for H_2^+ formation. Similar to the deprotonation channel, the isotropy arises from a long-lived intermediate induced by a conical intersection. Potential energy surface analysis[31,33] indicates that the dissociation proceeds via coupling of the $^{1,3}B_{1g}$ and $^{1,3}B_{1u}$ states to the lower-lying $^{1,3}B_{2u}$ state through a conical intersection, which creates a shallow potential well that stabilizes the dication. This extends the dissociation timescale beyond the rotational period of the dication, thereby erasing any directional preference induced by the laser polarization and resulting in an isotropic fragment distribution.

The symmetric dissociation channel corresponds to C–C bond rupture in the dication: $C_2H_4^{2+} \rightarrow CH_2^+ + CH_2^+$. Figures 4(a) and 4(b) show the measured KER spectra at peak intensities of 1×10^{14} W/cm^2 and 8×10^{14} W/cm^2, respectively; for comparison, Fig. 4(c) reproduces the distribution reported by Xie *et al.*[38] at 2×10^{15} W/cm^2. Multi-peak fits to the experimental spectra yield the KER peak positions and relative weights discussed below. By performing multi-peak fitting of the experimental data, the peak positions and distributions of the KER were obtained. At different laser densities in this study, the angular distribution of CH_2^+ ions is anisotropic, consistent with previous experimental results.[38]

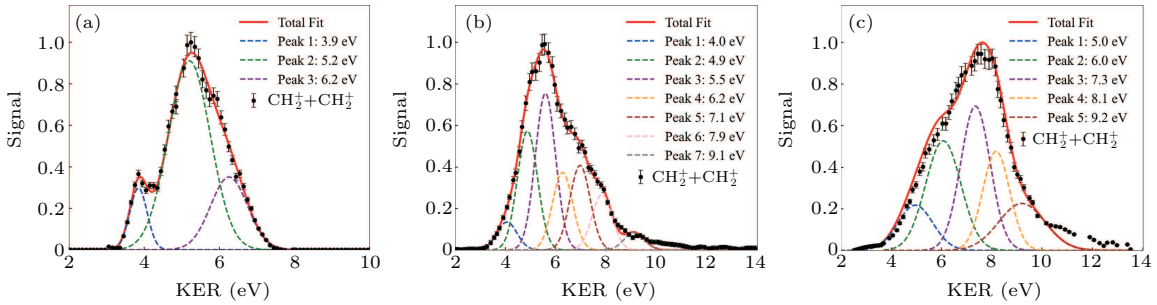


Fig. 4. Dissociation channels of $CH_2^+ + CH_2^+$: (a) KER spectrum corresponding to 1×10^{14} W/cm^2; (b) KER spectrum corresponding to 8×10^{14} W/cm^2; (c) KER spectrum corresponding to 2×10^{15} W/cm^2.

Under a laser intensity of 1×10^{14} W/cm^2, the KER spectrum in Fig. 4(a) is primarily centered around 5.2 eV, with weaker features at 3.9 eV and 6.2 eV. The C_2H_4 molecule forms the $^3B_{3u}$ state upon removal of electrons from the HOMO–2 and HOMO orbitals. Consequently, the main KER peak for symmetric dissociation is observed at 5.2 eV in the present experiment. This finding is supported by the analysis of the potential energy curves in Fig. 5(a), which shows that dissociation from the $^3B_{3u}$ state yields a theoretical KER of 5.0 eV,[31] in excellent agreement with the measurement. In addition, the peak at 6.2 eV in the KER spectrum corresponds to the dissociation channel of the $^3B_{3g}$ electronic state. Theoretical calculations yield a KER of 6.0 eV for this state, consistent with the experimental value. The dissociation mechanism is as follows: the dication is initially populated in the $^3B_{3g}$ state, which features a shallow potential well near the Franck–Condon region; as the C–C bond stretches, the system undergoes a conical intersection from the $^3B_{3g}$ state to the $^3B_{3u}$ state, and finally dissociates via the $^3B_{3u}$ state. Notably, prior studies of this channel did not report a peak at 3.9 eV; here we observe it for the first time and attribute it to the ^1A_u (S_2) state, for which theoretical calculations yield a KER value of 4.0 eV. In this pathway, removal of one HOMO and one HOMO–1 electron prepares ^1A_u (S_2). Subsequently, due to a conical intersection between the ^1A_u (S_2) and ^1A_g (S_1) states, the ion subsequently transfers from ^1A_u (S_2) to ^1A_g (S_1), from which the final dissociation occurs.

When the laser power density is increased to 8×10^{14} W/cm^2, the main peak appears at 6.2 eV. Under these conditions, the population of low-energy KER peaks with theoretical values of 4.0 eV, 5.0 eV, and 5.5 eV gradually decreases, while that of higher-energy KER peaks at 7.3 eV, 8.0 eV, and 9.0 eV correspondingly increases. The dissociation mechanisms of the low-energy KER peaks (4.0 eV, 5.0 eV, and 5.5 eV) and the main peak (6.2 eV) are consistent with those at lower laser power densities. Specifically, the 4.0 eV KER peak corresponds to the ^1A_u (S_2) state, the 5.0 eV and 5.5 eV peaks arise from the $^3B_{3u}$ and $^3B_{3g}$ states, respectively, while the main peak at 6.2 eV originates from the crossing dissociation channel involving the $^3B_{3g} \rightarrow ^3B_{3u}$ transition. Of particular interest is a 7.1 eV peak that arises from population on $^3B_{1u}$, which transfers via conical intersections to $^3B_{1g}$ before dissociation.[38] Its calculated KER is 7.3 eV. In addition, double ionization from the HOMO–2 orbital populates the highly excited 3^1A_g state of $C_2H_4^{2+}$, which directly induces C–C bond cleavage. The experimentally observed KER

peaks at 7.9 eV and 9.1 eV correspond to dissociation via the 3^1A_g state following conical intersections to the $^1B_{3g}$ and 2^1A_g states, respectively. The associated theoretical values are 8.0 eV and 9.0 eV, in excellent agreement with the experimental data. When the laser power density is further increased to 2×10^{15} W/cm^2, the main peak shifts to 7.3 eV, the population of low-energy KER peaks is further suppressed, and high-energy KER peaks become dominant. Importantly, the KER peaks at 8.1 eV and 9.2 eV observed under this condition exhibit dissociation mechanisms that are fundamentally different from the peaks at the same energies under lower power densities.[38] These peaks arise from low-lying 1^1A_g states that are promoted via field-induced excitation to the highly excited 3^1A_g state, which subsequently undergoes conical intersections to the 2^1A_g and $^1B_{3g}$ states and then dissociates along these high-lying pathways. Consequently, the theoretical KER values for this process are the same as those of the corresponding dissociation pathways at lower power densities. To provide an intuitive illustration of how the dissociation pathways of different electronic states depend on the laser power density, Fig. 5(b) presents the populations of various electronically excited states of $C_2H_4^{2+}$ as a function of laser power density. At low power density (1×10^{14} W/cm^2), the lower excited states $^3B_{3u}$ and $^3B_{3g}$ dominate ($\sim 90\%$), while the even lower ^1A_u (S_2) state is also populated ($\sim 10\%$). This indicates that, within this intensity regime, the laser field primarily ionizes the outer-valence electrons of C_2H_4, and the resulting dissociation channels correspond to the potential energy surfaces of relatively low-lying excited states. As the laser power density increases to 8×10^{14} W/cm^2, the populations of the excited states undergo significant changes: the ^1A_u (S_2) state drops sharply to approximately 5%, while the $^3B_{3u}$ and $^3B_{3g}$ states decrease to around 65%. At the same time, higher-lying excited states ($^3B_{1u}$, 3^1A_g) begin to be significantly populated. This shift indicates that, at intermediate power densities, the laser field possesses sufficient energy to ionize inner-valence electrons, generating highly excited states via removal of these inner electrons. At a laser power density of 2×10^{15} W/cm^2, the ^1A_u (S_2) state nearly vanishes, and the populations of lower excited states such as $^3B_{3u}$ and $^3B_{3g}$ decrease to about 37%. This indicates that their efficiency as dissociation channels is strongly suppressed, primarily due to the competitive population of higher-lying states. At this laser power density, the dissociation process is dominated by higher excited states including $^3B_{1u}$ and 3^1A_g. The formation mechanism of these states shifts from being governed mainly by direct ionization to being driven predominantly by field-induced excitation — namely, ions in lower excited states absorb additional photons in the intense laser field and are promoted to higher electronic states. These results indicate that increasing laser power density drives a transition from low-energy ionization-driven channels to high-energy excitation-dominated dissociation pathways. In summary, the peak laser power density is the key factor controlling the relative yields of different dissociation pathways. At intensities of 1×10^{14} W/cm^2 or below, $C_2H_4^{2+}$ predominantly populates the $^3B_{3u}$ state, with a relatively large contribution from the ^1A_u (S_2) state. As the intensity increases, population channels leading to the 3^1A_g and $^3B_{1u}$ states become accessible. With further increase in intensity, field-induced excitation to the 3^1A_g and $^3B_{1u}$ high-lying states becomes dominant. The dissociation pathways of C_2H_4 can thus be actively manipulated by precise adjustment of the laser power density: on the one hand, selective ionization of different orbitals determines the initial excited states and their dissociation channels (e.g., low intensities ionize outer-valence HOMO and HOMO–1 to produce low-lying states, whereas high intensities ionize the deeper HOMO–2 to generate higher-lying states); on the other hand, at high intensities, field-induced excitation can promote $C_2H_4^{2+}$ from low-lying to higher excited states, thereby substantially altering the subsequent dissociation dynamics. Therefore, the laser power density serves as the critical experimental parameter for steering molecular dissociation pathways.

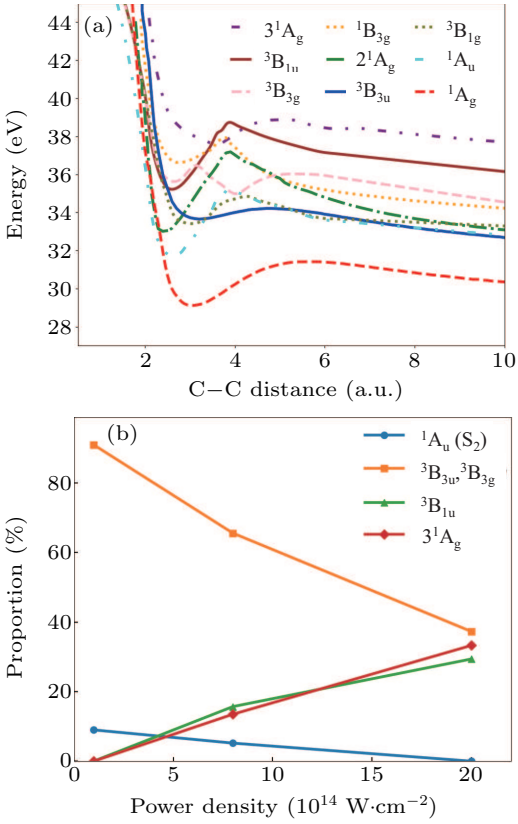


Fig. 5. (a) Calculated potential energy curves of $C_2H_4^{2+}$ along the C–C stretching coordinate.[31] (b) Population fractions of electronically excited states as a function of laser intensity.

4. Conclusion

This work investigates the mechanisms of two-body dissociative fragmentation of $C_2H_4^{2+}$ induced by strong laser

fields at different power densities using momentum coincidence imaging. All two-body Coulomb explosion dissociation channels of $C_2H_4^{2+}$ within the studied laser intensity range are identified. Particular emphasis is placed on the laser-intensity-dependent control of the symmetric dissociation pathway ($CH_2^+ + CH_2^+$), in which a new KER peak at 4 eV is observed for the first time and assigned to the ^1A_u (S_2) state.

Analysis of the potential energy curves indicates that the deprotonation channel originates from the ^3A_u (T_1) ionic state, while the dissociation process of the $C_2H_4^{2+} \rightarrow C_2H_2^+ + H_2^+$ channel proceeds via coupling between the $^{1,3}B_{1g}$ and $^{1,3}B_{1u}$ states, followed by relaxation to the lower-lying $^{1,3}B_{2u}$ state through a conical intersection.

For the symmetric dissociation channel of $C_2H_4^{2+}$, the KER spectra exhibit pronounced evolution with increasing laser power density: the main feature shifts from a low-energy peak (5.2 eV) to dominant high-energy peaks (7.3–9.0 eV). This behavior reflects a transition in the dominant dissociation mechanism. At low laser intensities, selective ionization of specific molecular orbitals populates low-lying dissociative states (e.g., ^1A_u (S_2), $^3B_{3u}$), whereas at higher intensities, field-induced excitation promotes the dication to higher-lying dissociative states (e.g., 3^1A_g, $^3B_{1u}$).

Correlation analysis of electronic-state populations at different power densities demonstrates that the peak laser power density is the key parameter governing the dissociation mechanism, as it directly determines the relative contributions of different channels. By precisely tuning the laser parameters to selectively populate target ionic states, specific dissociation pathways can be enhanced or suppressed. This study elucidates the pathway-selection mechanism in strong-field double ionization of ethylene, governed by the complex population dynamics of electronic states, and highlights the potential of femtosecond laser intensity as a powerful tool for steering dissociation pathways in polyatomic molecules.

Acknowledgments

This work was supported by the National Natural Science Foundation of China (Grant Nos. 12304376, 12504397, and 12204132), the Shandong Provincial Natural Science Foundation (Grant Nos. ZR2025QC1459, TSQN202408113, and ZR2023QA075), and the National Key Research and Development Program of China (Grant No. 2022YFA1602500).

References

[1] Song M Y, Yoon J S, Cho H, Karwasz G P, Kokoouline V, Nakamura Y and Tennyson J 2017 *J. Phys. Chem. Ref. Data* **46** 013106
[2] Hosaka K, Yokoyama A, Yamanouchi K and Itakura R 2013 *J. Chem. Phys.* **138** 204301
[3] Naikoo G A, Arshad F, Hassan I U, Tabook M A, Pedram M Z, Mustaqeem M, Tabassum H, Ahmed W and Rezakazemi M 2021 *Front. Chem.* **9** 736801
[4] Watanabe N and Takahashi M 2023 *Phys. Rev. A* **108** 042814
[5] Das R, Pandey D K, Soumyashree S, Madhusudhan P, Nimma V, Bhardwaj P, Shameem M K M, Singh D K and Kushawaha R K 2022 *Phys. Chem. Chem. Phys.* **24** 18306
[6] Zhang W, Gong X, Li H, Lu P, Sun F, Ji Q, Lin K, Ma J, Li H and Qiang J 2019 *Nat. Commun.* **10** 757
[7] Zhang W, Yu Z, Gong X, Wang J, Lu P, Li H, Song Q, Ji Q, Lin K and Ma J 2017 *Phys. Rev. Lett.* **119** 253202
[8] Sun R and Xin P 2024 *Phys. Scr.* **99** 105412
[9] Hu C X, Li W Z, Zhang W B, Gong X C, Wu J and He F 2021 *Phys. Rev. A* **103** 043122
[10] Wang Y, Lai X, Yu S, Sun R, Liu X, Dorner-Kirchner M, Erattupuzha S, Larimian S, Koch M and Hanus V 2020 *Phys. Rev. Lett.* **125** 063202
[11] Jin W, Wang C, Zhao X, Yang Y, Ren D, Liu Z, Li X, Luo S and Ding D 2024 *Chin. Phys. Lett.* **41** 053101
[12] Richard B, Boll R, Banerjee S, Schäfer J M, Jurek Z, Kastirke G, Fehre K, Schöffler M S, Anders N and Baumann T M 2025 *Science* **389** 650
[13] Yao H, Guo W, Hoffmann M R and Han K 2014 *Phys. Rev. A* **90** 063418
[14] Brun F, Ribotte L, Boutoux G, Davoine X, Masson-Laborde P, Sentoku Y, Iwata N, Blanchot N, Batani D and Lantuéjoul I 2024 *Matter Radiat. Extremes* **9** 057203
[15] Chen L, Shan X, Wang E, Ren X, Zhao X, Huang W and Chen X 2019 *Phys. Rev. A* **100** 062707
[16] Xie H B, Li C, He N, Wang C, Zhang S and Chen J 2014 *Environ. Sci. Technol.* **48** 1700
[17] Pan S, Hu C, Zhang Z, Lu P, Lu C, Zhou L, Wang J, Sun F, Qiang J and Li H 2022 *Ultrafast Sci.* **2022** 9863548
[18] Li X, Boll R, Vindel-Zandbergen P, González-Vázquez J, Rivas D E, Bhattacharyya S, Borne K, Chen K, De Fanis A and Erk B 2025 *Nat. Commun.* **16** 7006
[19] Liu Y R, Bai X, Nan Q W, Kimberg V, Gong M, Yang Y K, Cheng Y, Chen J, Vendrell O and Ueda K 2025 *Commun. Phys.* **8** 331
[20] Kling M F, Von Den Hoff P, Znakovskaya I and de Vivie-Riedle R 2013 *Phys. Chem. Chem. Phys.* **15** 9448
[21] Rathje T, Sayler A, Zeng S, Wustelt P, Figger H, Esry B and Paulus G 2013 *Phys. Rev. Lett.* **111** 093002
[22] Kinugawa T, Lablanquie P, Penent F, Palaudoux J and Eland J 2004 *J. Electron. Spectrosc. Relat. Phenom.* **141** 143
[23] Xie X, Doblhoff-Dier K, Roither S, Schöffler M S, Kartashov D, Xu H, Rathje T, Paulus G G, Baltuška A and Gräfe S 2012 *Phys. Rev. Lett.* **109** 243001
[24] Znakovskaya I, von Den Hoff P, Zherebtsov S, Wirth A, Herrwerth O, Vrakking M J, de Vivie-Riedle R and Kling M F 2009 *Phys. Rev. Lett.* **103** 103002
[25] Lezius M, Blanchet V, Ivanov M Y and Stolow A 2002 *J. Chem. Phys.* **117** 1575
[26] Markevitch A N, Smith S M, Romanov D A, Schlegel H B, Ivanov M Y and Levis R J 2003 *Phys. Rev. A* **68** 011402
[27] Appell J, Durup J, Fehsenfeld F and Fournier P 1974 *J. Phys. B: Atom. Mol. Phys.* **7** 406
[28] Fournier P, Fournier J, Langford M and Harris F 1993 *Chem. Phys.* **178** 581
[29] Rye R, Madey T, Houston J and Holloway P 1978 *J. Chem. Phys.* **69** 1504
[30] Thompson M, Hewitt P A and Wooliscroft D S 1976 *Anal. Chem.* **48** 1336
[31] Gaire B, Lee S, Haxton D, Pelz P, Bocharova I, Sturm F, Gehrken N, Honig M, Pitzer M and Metz D 2014 *Phys. Rev. A* **89** 013403
[32] Jochim B, Erdwien R, Malakar Y, Severt T, Berry B, Feizollah P, Rajput J, Kaderiya B, Pearson W and Carnes K 2017 *New J. Phys.* **19** 103006
[33] Wang B, Wei L, Zhang Y, Yu W, Zou Y, Chen L and Wei B 2020 *J. Phys. B* **53** 155205
[34] Kalugina Y N, Cherepanov V N, Buldakov M A, Zvereva-Loëte N and Boudon V 2012 *J. Comput. Chem.* **33** 319
[35] Luo D, Wei B, Zhang Y, Zou Y, Hutton R, Chen F and Wang X 2018 *J. Phys. B* **51** 165203
[36] Song Q, Gong X, Ji Q, Lin K, Pan H, Ding J, Zeng H and Wu J 2015 *J. Phys. B* **48** 094007
[37] Guo C, Li M, Nibarger J P and Gibson G N 1998 *Phys. Rev. A* **58** R4271
[38] Xie X, Roither S, Schöffler M, Lötstedt E, Kartashov D, Zhang L, Paulus G G, Iwasaki A, Baltuška A and Yamanouchi K 2014 *Phys. Rev. X* **4** 021005